Volume 61
Number 21
14 March 2025
Pages 4081–4254

ChemComm

Chemical Communications

rsc.li/chemcomm

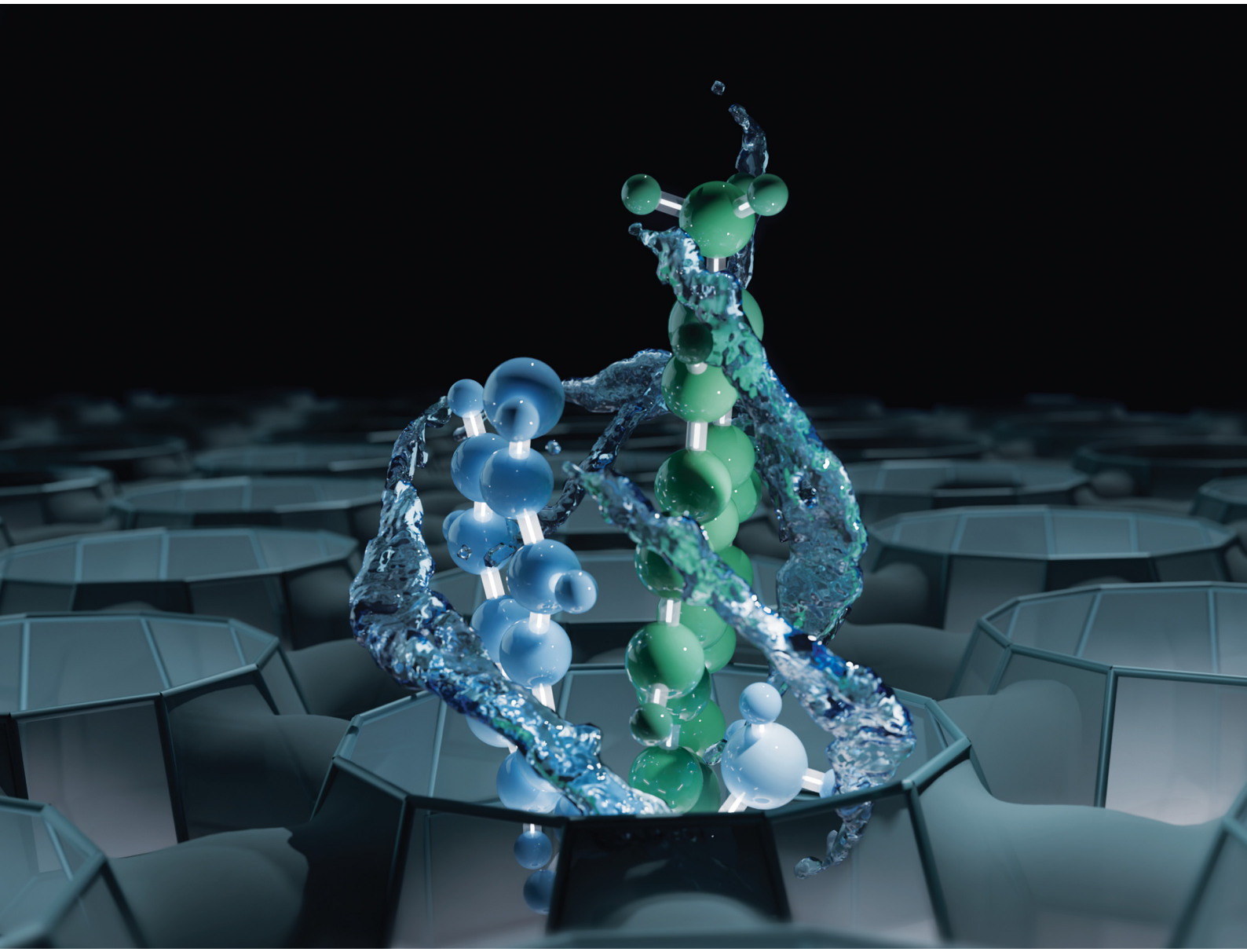

ISSN 1359-7345

ROYAL SOCIETY OF CHEMISTRY

COMMUNICATION

Frank Biedermann, Ettore Fois, Gloria Tabacchi *et al.*
Mechanistic insights into water-stabilized dye-neurotransmitter intermolecular complexes in zeolite channels

ChemComm

COMMUNICATION

View Article Online
View Journal | View Issue

Cite this: *Chem. Commun.*, 2025, **61**, 4160

Received 9th November 2024,
Accepted 15th January 2025

DOI: 10.1039/d4cc05980h

rsc.li/chemcomm

Mechanistic insights into water-stabilized dye-neurotransmitter intermolecular complexes in zeolite channels†

Cristiano Invernizzi,[a] Laura M. Grimm,[b] Frank Biedermann,*[b] Ettore Fois*[a] and Gloria Tabacchi*[a]

Dye-zeolite nanomaterials are promising candidates for neurotransmitter detection, however, their sensing mechanism has remained speculative. Using *ab initio* molecular dynamics (AIMD) simulations, we demonstrate that water molecules play a critical role in stabilizing complexes formed between the dicationic dye and cationic neurotransmitters within the zeolite framework. This interaction exhibits binding motifs akin to those in protein–ligand complexes rather than conventional host–guest systems. Furthermore, the presence of water significantly modulates the spectroscopic properties of the nanosensor.

Molecular recognition in aqueous environments is a complex, multifaceted process influenced not only by direct molecular interactions but also by the unique role of water as a structure-directing agent. Hydrophobic effects and the capacity of water molecules to bridge interacting species play a central role in mediating these interactions. In protein–ligand complexes, water molecules in the hydration shell can significantly affect both the thermodynamics and kinetics of recognition events, acting as structural templates that can either promote or inhibit binding, depending on water arrangement near binding sites.[1] This water-mediated organization, which is critical in natural systems, suggests that water molecules can either bridge or displace upon ligand binding, thereby influencing the overall binding affinity and specificity.[2]

In contrast, our understanding of water's role in molecular recognition within artificial receptors and material-based systems remains limited. Macrocyclic hosts such as cucurbit[*n*]urils, calix[*n*]arenes, and cyclodextrins, while widely used in host–guest chemistry, typically possess hydrophobic cavities that lack anchoring points for structured water. Consequently, partial or complete de-wetting of the cavity often occurs, particularly with larger organic guests.[3] This de-wetting process can limit the binding affinities and selectivities of these hosts, marking a notable contrast to protein–ligand complexes, where structured water plays a pivotal role in facilitating molecular recognition. While structured water is sometimes observed in the solid-state structures of these systems,[4] it does not significantly influence their binding characteristics. In this regard, current synthetic receptors lack the capacity to replicate this critical feature of molecular recognition observed in proteins.

Recently, we showed that hybrid organic–inorganic materials composed of microporous zeolites loaded with a fluorescent dicationic dye as a cofactor exhibit remarkable affinity and selectivity for binding the neurotransmitter serotonin. The sensing was achieved by the appearance of new bands in the optical spectra of the receptor when titrated with the neurotransmitter.[5] These straightforward "nanosensors," self-assembled simply by mixing an aqueous dispersion of zeolite with a dye solution, outperform other synthetic receptors across key binding parameters. Using spectroscopic and calorimetric analyses, we identified the direct interactions between the dye and the neurotransmitter, as well as between the neurotransmitter and the zeolite, as essential contributors to the exceptionally high binding affinity and selectivity observed. Computational analyses using a static density functional theory (DFT) model initially seemed sufficient to elucidate the origin of the new bands in the optical spectra.[5] However, these calculations did not explicitly account for the presence of water or the zeolite framework, which are key components of the experimental system.[5] Furthermore, the static DFT results did not explain the experimentally observed spectral differences compared to host–guest complexes with cucurbit[8]uril (CB8), where the same dye and analyte form a well-defined face-to-face stacking arrangement within the cavity.[6] Consequently, we

[a] *Department of Science and High Technology, Insubria University and INSTM, via Valleggio 11, 22100 COMO, Italy. E-mail: ettore.fois@uninsubria.it, gloria.tabacchi@uninsubria.it*
[b] *Institute of Nanotechnology, Karlsruhe Institute of Technology (KIT), Hermann-von-Helmholtz Platz 1, 76344 Eggenstein-Leopoldshafen, Germany. E-mail: frank.biedermann@kit.edu*

† Electronic supplementary information (ESI) available: Details of the computational procedures, simulated UV-vis spectra, radial distribution functions, MDAP_SERO_ZL.mpeg movie on the dynamics of the (MDAP + SERO)ZL system. See DOI: https://doi.org/10.1039/d4cc05980h

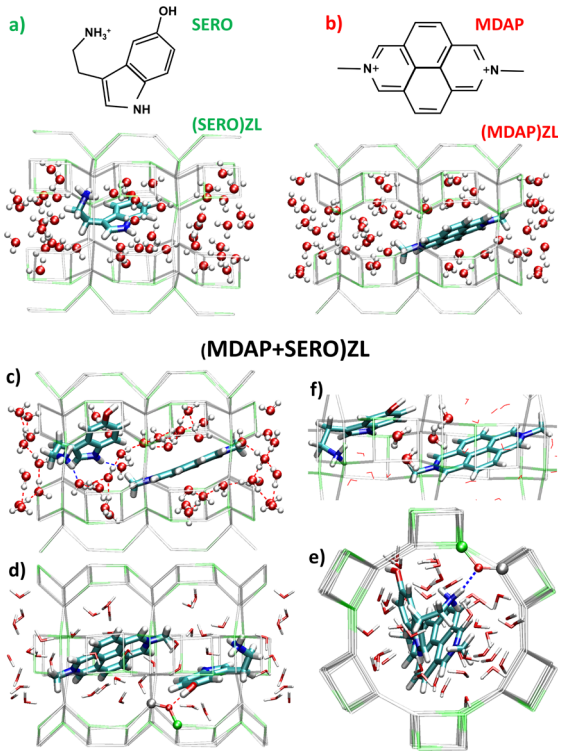

Fig. 1 (a) and (b) Minimum energy configurations of (SERO)ZL and (MDAP)ZL; (c)–(f) Representations of the (MDAP + SERO)ZL minimum energy structure highlighting: (c) the hydrophobic solvation shell of zeolitic water around MDAP; (d) and (e) H-bonds between SERO –OH/–NH_3^+ groups and ZL oxygen atoms; (f) four water molecules positioned between MDAP and SERO. Color code: gray = Si, green = Al, red = O, cyan = C, blue = N, white = H; H-bonds are shown as dashed lines. Framework O atoms and extraframework K^+ are not shown for clarity.

hypothesized that incorporating explicit water molecules, the zeolite framework, and their dynamic interactions into the computational model would provide deeper insights into the binding and sensing mechanism and account for the features observed experimentally.

Here, we explored these effects by building periodic atomistic models of the zeolite-based nanosensors and evaluating their properties under both static and dynamic conditions in the presence of explicit water molecules. The host matrix was negatively charged zeolite L (ZL; ESI,† S1.1), paired with the dicationic dye 2,7-dimethyldiazapyrenium (MDAP) and the cationic neurotransmitter serotonin (SERO) (Fig. 1). We focused on three model systems: (SERO)ZL, the host–guest complex of SERO with the parent ZL material (Fig. 1a); (MDAP)ZL, the nanosensor in the absence of serotonin (Fig. 1b), and (MDAP + SERO)ZL – a complex of MDAP and SERO in ZL, mimicking the nanosensor with serotonin included (Fig. 1c–f). To rigorously study these systems, we conducted DFT-based geometry optimizations and AIMD simulations, using a setup validated for similar zeolite host–guest systems[7] (ESI,† S1.2). This approach enabled us to capture the dynamic behavior of water and assess its influence on binding within ZL framework, marking a shift from prior static models and providing a comprehensive view of the molecular recognition mechanism at play.

The minimum energy structures of the three models (Fig. 1) show that the organic guests – whose π-conjugated systems are planar– are embedded in the H-bond network of zeolitic water. MDAP – having no H-bonding sites – occupies the centre of the ZL channel irrespective of SERO presence (Fig. 1b and c). Water molecules form a hydrophobic solvation shell around MDAP, with their oxygen atoms all pointing toward MDAP (Fig. 1b and c). This behaviour aligns with previous observations for other dyes in zeolitic pores.[8] SERO is anchored to the ZL channel wall *via* two strong H-bonds (with the –NH_3^+ and –OH groups) – involving two negatively charged AlO_4 ZL units (Fig. 1d and e). Hence, SERO is only partially solvated by water independently of MDAP presence. SERO forms supramolecular complexes with MDAP, with shortest intermolecular distance of 3.2 Å. Four H_2O molecules are situated between the organic guests, acting as a dielectric buffer that screens the repulsive interactions between the cations (Fig. 1f). Thus, along with the charge-balancing and space-confining effects of the ZL channel, even water plays a key role in stabilizing this triply charged supramolecular complex.

UV-vis spectra were calculated by time-dependent DFT[9a] on cluster models (Fig. 2a–c) extracted from the minimum energy structure of the three systems. In the clusters, MDAP and SERO were treated at the CAM-B3LYP[9b]/6-311++G(df,pd) level, while a point-charge model[9c] was adopted for H_2O (ESI,† S1.3 and S1.4). The spectrum of the MDAP + SERO complex is compared with the MDAP and SERO ones in Fig. 2d (see also ESI,† S4.1 and S4.2). Close inspection revealed two low-intensity bands at 457 nm and 414 nm, assigned to HOMO → LUMO and HOMO−1 → LUMO excitations, respectively (Fig. 2d, inset). While HOMO and HOMO−1 are localized on SERO, the LUMO is centered on MDAP (Fig. 2e, insets). These excitations – absent in the spectra of MDAP and SERO – correspond to SERO-to-MDAP charge-transfer (CT) transitions, as proposed in ref. 5.

Until now, we have focused on the minimum energy properties of the systems (*i.e.*, at 0 K). The dynamics of (MDAP + SERO)ZL is illustrated in the enclosed movie (Movie S1, MDAP_SERO_ZL.mpeg, ESI,† S8). To assess thermal effects, we examined room-temperature trajectories *via* radial distribution functions ($g(r)$s), which offer an averaged structural perspective of the three host–guest complexes (see ESI,† S5 for details). This analysis revealed strong H_2O–H_2O H-bonding and a quasi-liquid H_2O structure in all systems (Fig. S22, ESI†). Water forms strong H-bonds with ZL oxygens (Fig. S23, ESI†) as well as with the SERO NH and –NH_3^+ protons (Fig. S24, ESI†). The H_2O-MDAP separation decreases in the presence of SERO (Fig. S27 and S28, ESI†), while the distance between the aromatic core hydrogens of MDAP (H_{ar}) and ZL oxygens shows minimal change from (MDAP)ZL to (MDAP + SERO)ZL. In contrast, the separation of MDAP –CH_3 protons from ZL oxygens slightly decreases (Fig. 3a), indicating weak MDAP-ZL interactions. Importantly, the SERO –NH_3^+ group and aromatic moiety approach the ZL walls in the presence of MDAP (Fig. 3b), suggesting a stronger affinity of SERO for nanosensor than for parent ZL, consistent with experimental findings.[5]

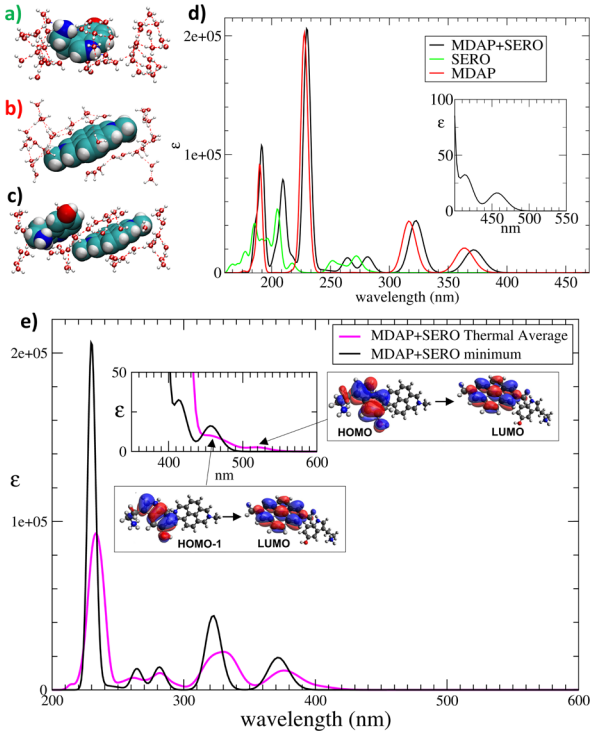

Fig. 2 (a)–(c) Cluster models extracted from the minimum energy structures of (a) (SERO)ZL; (b) (MDAP)ZL; (c) (MDAP + SERO)ZL. MDAP, SERO: large spheres, H_2Os: ball-and-stick. (d) UV-vis spectra calculated for cluster models (a)–(c); (e) comparison of UV-vis spectrum of cluster (c) with the thermally averaged spectrum, obtained from analogous cluster models cut from configurations sampled along (MDAP + SERO)ZL trajectory. Insets: CT bands (457 nm and 414 nm for the minimum; 520 nm and 460 nm for the thermal average) and the involved MOs.

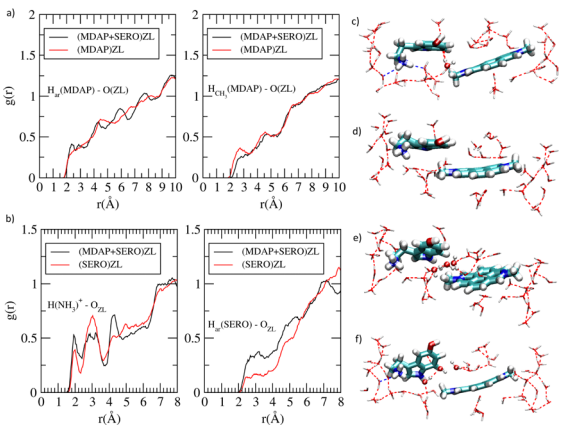

Fig. 3 Radial distribution functions $g(r)$'s for (a) MDAP aromatic protons (H_{ar}) and methyl protons (H_{CH_3}) with ZL oxygens, (b) SERO $-NH_3^+$ protons and aromatic protons (H_{ar}) with ZL oxygens. (c)–(f) cluster models extracted from 4 configurations of (MDAP + SERO)ZL AIMD simulation, with different MDAP/SERO distortions, orientations, and H_2O arrangements. The H_2Os located between MDAP and SERO in (c), (e), and (f) are in ball-and-stick. Colors as in Fig. 1.

Thermally-averaged spectra were calculated on cluster models formed by the organic species and the surrounding H_2O (see Fig. 3c–f for representative examples), extracted from configurations sampled along the AIMD trajectories (ESI,† S6). The bands in the thermally averaged spectrum are broader and red-shifted compared to the 0 K spectrum (Fig. 2e). This red shift is particularly significant for the CT bands, which now appear as a broad tail in the 450–550 nm region (Fig. 2e, inset), in line with experiments.[5] The signals corresponding to the HOMO → LUMO and HOMO−1 → LUMO CT transitions are at 520 nm and 460 nm, respectively (Fig. 2e). Such CT bands were at 457 nm and 414 nm in the minimum structure, indicating a key role of thermal effects in red-shifting CT transitions.

The atomistic factors affecting the CT excitations were examined by analyzing key geometrical parameters: (i) the conformation of SERO, (ii) the distortion from planarity of the π-structures, (iii) the relative orientation of MDAP and SERO, (iv) the MDAP–SERO separation, and (v) the number of H_2O situated between MDAP and SERO. Configurations in which MDAP and SERO adopt an "edge-to-face" arrangement (Fig. 3e and f) or a nearly planar geometry of the π-systems (Fig. 3c) show a red shift in the HOMO → LUMO CT band, independent of SERO conformation. Conversely, configurations with large deviations from planarity in the π-systems of SERO or MDAP (Fig. 3d) present a blue shift of the HOMO → LUMO CT band. This suggests that factors (ii) and (iii) are key determinants of the CT wavelength, though their effect on intensity is less pronounced. The CT band intensity is modestly higher in configurations with edge-to-face MDAP–SERO orientations and near-planar π-systems than in other configurations. Parameters (iv) and (v) were found to be interdependent: in configurations with only one or no H_2O between the guests (Fig. 3c and d), the MDAP–SERO separation is shorter than in the minimum-energy structure, while when multiple H_2Os are situated between MDAP and SERO (Fig. 3e and f), the separation increases. Notably, configurations with shorter MDAP–SERO distance display increased oscillator strength of the CT bands, indicating that H_2O plays a crucial role in tuning both the SERO-MDAP separation and the CT band intensity. In a first summary, thermal motion shifts the energy of the CT bands, but their intensity remains low, implying that additional factors may influence this quantity.

Thus far, the ZL host has not been included in the spectral calculations. As a next step, we examined the effect of the ZL matrix, modeled as a point-charge system[10] (Fig. 4a and b and ESI,† S1.4), on the CT bands in the minimum energy structures of (MDAP)ZL and (MDAP + SERO)ZL. This approach allows us to isolate the influence of the ZL host from the previously discussed thermal effects. A comparison of the spectra with and without the ZL inclusion is shown in Fig. 4c. The ZL host has a minimal impact on the MDAP spectrum, causing only a slight shift in the longest-wavelength bands (Fig. 4c and ESI,† S7.1). In contrast, the effect of the ZL framework is more pronounced for the MDAP + SERO complex (Fig. 4c and ESI,† S7.2). Notably, ZL inclusion substantially increases the CT band intensity. The HOMO → LUMO intensity grows by nearly an order of magnitude (Table S3, ESI†), although its position remains unchanged. Even the HOMO−1 → LUMO intensity grows significantly, with a slight blue shift (from 414 to 395 nm). The greater effect of ZL on the MDAP + SERO spectrum compared to the MDAP one can be attributed to the strong H-bonds formed between SERO's $-NH_3^+$ and –OH groups and the ZL oxygens. As a result,

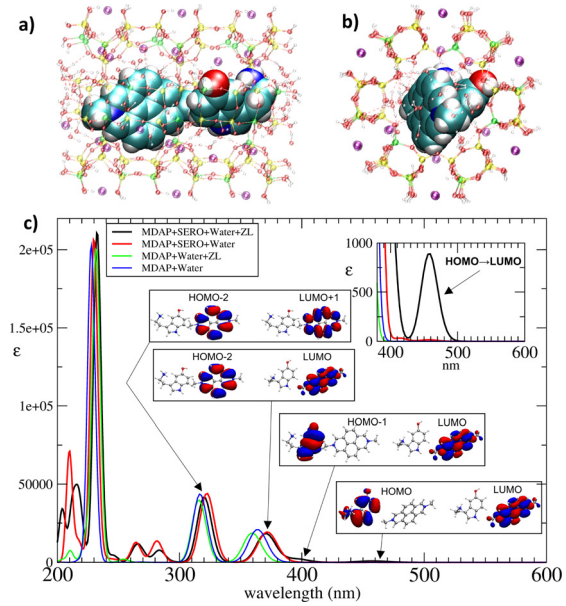

Fig. 4 (a) and (b) Two orientations of the cluster model used to calculate the UV-vis spectrum of MDAP + SERO in ZL. Color code: yellow = Si, green = Al, red = O, cyan = C, blue = N, white = H; purple: K^+; (c) comparison of the UV-vis spectra obtained from cluster models cut from the minimum energy structures of (MDAP + SERO)ZL and (MDAP)ZL with the inclusion of ZL framework and without ZL framework. Insets: MOs involved in the CT bands and in the two longest wavelength bands localized on MDAP.

solvation by H_2O alone may not fully shield the MDAP + SERO complex from interactions with ZL atoms. The anchoring of SERO cation to the negatively charged ZL walls likely enhances its electron-donating capacity upon excitation, strengthening charge transfer toward the nearby electron acceptor, the MDAP dication reporter.

This interaction results in an increased intensity of CT excitations. Importantly, the two CT bands account for the long-wavelength tail observed in the (MDAP)ZL optical spectra upon titration with SERO.[5] This finding indicates that host–guest interactions—particularly the direct binding of SERO to ZL—are central to the nanoreceptor's sensing mechanism.[5] This insight suggests opportunities to enhance nanosensor performance by optimizing the pairing of the zeolite host and reporter dye based on the target analyte. Specifically, in addition to forming a confined analyte-dye CT complex (ESI,† S4.4), strong interactions between the analyte cation and the negatively charged host are essential to maximize the CT signal intensity.

In conclusion, we have modeled the dynamic behavior of nanosensors based on ZL and MDAP for detecting SERO. Our analysis connects specific conformations of the MDAP + SERO complex within ZL channels to the detailed structure of the experimental spectroscopic signal. Notably, we identified the key factors enhancing CT band intensity: (i) a reduced MDAP–SERO distance, (ii) an edge-to-face arrangement of the SERO and MDAP π-systems, and (iii) minimal distortions from planarity in the π-systems. Our approach demonstrates the significant impact of the electrostatic field generated by the ZL host on the spectroscopic properties of confined cationic complexes. Furthermore, incorporating the dynamic behavior of water in the zeolite cavity provides a deeper understanding of the binding mechanism, revealing the crucial balance between framework interactions and water-mediated interactions, at difference with static DFT models. Such insights will guide the design of future synthetic receptors and materials, harnessing water's dual role in enhancing and modulating molecular recognition processes in aqueous environments.

Insubria University (FAR2023) financed this work.

Data availability

The data supporting this paper are included in the ESI.†

Conflicts of interest

There are no conflicts to declare.

Notes and references

1 (*a*) Y. Levy and J. N. Onuchic, *Proc. Natl. Acad. Sci. U.S.A.*, 2004, **101**, 3325; (*b*) E. A. Meyer, R. K. Castellano and F. Diederich, *Angew. Chem., Int. Ed.*, 2003, **42**, 1210; (*c*) G. Klebe, *Nat. Rev. Drug Discovery*, 2015, **14**, 95.
2 J. E. Ladbury, *Chem. Biol.*, 1996, **3**, 973.
3 (*a*) W.-B. Hu, W.-J. Hu, Y. A. Liu, J.-S. Li, B. Jiang and K. Wen, *Chem. Commun.*, 2016, **52**, 12130; (*b*) L.-P. Yang, X. Wang, H. Yao and W. Jiang, *Acc. Chem. Res.*, 2020, **53**, 198; (*c*) L.-P. Yang, L. Zhang, M. Quan, J. S. Ward, Y.-L. Ma, H. Zhou, K. Rissanen and W. Jiang, *Nat. Commun.*, 2020, **11**, 2740; (*d*) F. Biedermann, W. M. Nau and H.-J. Schneider, *Angew. Chem., Int. Ed.*, 2014, **53**, 11158.
4 C. Rando, J. Vázquez, J. Sokolov, Z. Kokan, M. Nečas and V. Šindelář, *Angew. Chem., Int. Ed.*, 2022, **61**, e202210184.
5 L. M. Grimm, S. Sinn, M. Krstić, E. D'Este, I. Sonntag, E. A. Prasetyanto, T. Kuner, W. Wenzel, L. De Cola and F. Biedermann, *Adv. Mater.*, 2021, **33**, 2104614.
6 (*a*) F. Biedermann and W. M. Nau, *Angew. Chem., Int. Ed.*, 2014, **53**, 5694; (*b*) F. Biedermann, G. Ghale, A. Hennig and W. M. Nau, *Commun. Biol.*, 2020, **3**, 383.
7 (*a*) G. Tabacchi, *ChemPhysChem*, 2018, **19**, 1249; (*b*) L. Gigli, R. Arletti, G. Tabacchi, M. Fabbiani, J. G. Vitillo, G. Martra, A. Devaux, I. Miletto, S. Quartieri, G. Calzaferri and E. Fois, *J. Phys. Chem. C*, 2018, **122**, 3401; (*c*) E. Fois, G. Tabacchi, A. Devaux, P. Belser, D. Brühwiler and G. Calzaferri, *Langmuir*, 2013, **29**, 9188; (*d*) E. Fois and G. Tabacchi, in *Tailored Functional Oxide Nanomaterials: From Design to Multi-Purpose Applicationsm*, ed. C. Maccato and D. Barreca, Wiley-VCH GmbH, Weinheim, 2022, pp. 111–136; (*e*) E. Fois and G. Tabacchi, *Small Struct.*, 2024, 2400346, DOI: 10.1002/sstr.202400346; (*f*) G. Tabacchi, E. Fois and G. Calzaferri, *Angew. Chem., Int. Ed.*, 2015, **54**, 11112.
8 (*a*) R. Arletti, E. Fois, L. Gigli, G. Vezzalini, S. Quartieri and G. Tabacchi, *Angew. Chem., Int. Ed.*, 2017, **56**, 2105; (*b*) G. Tabacchi, G. Calzaferri and E. Fois, *Chem. Commun.*, 2016, **52**, 11195; (*c*) E. Fois and G. Tabacchi, *Z. Kristallogr. Cryst. Mater.*, 2019, **234**, 495; (*d*) M. Fischer, *Z. Kristallogr. Cryst. Mater.*, 2015, **230**, 325; (*e*) E. Fois, A. Gamba, C. Medici, G. Tabacchi, S. Quartieri, E. Mazzucato, R. Arletti, G. Vezzalini and V. Dmitriev, *Micropor. Mesopor. Mat.*, 2008, **115**, 267; (*f*) X. Zhou, T. A. Wesolowski, G. Tabacchi, E. Fois, G. Calzaferri and A. Devaux, *Phys. Chem. Chem. Phys.*, 2013, **15**, 159; (*g*) E. Fois, G. Tabacchi, S. Quartieri and G. Vezzalini, *J. Chem. Phys.*, 1999, **111**, 355.
9 (*a*) M. E. Casida, C. Jamorski, K. C. Casida and D. R. Salahub, *J. Chem. Phys.*, 1998, **108**, 4439; (*b*) T. Yanai, D. P. Tew and N. C. Handy, *Chem. Phys. Lett.*, 2004, **393**, 51; (*c*) R. J. Woods and R. Chappelle, *J. Mol. Struc.*, 2000, **527**, 149.
10 J. Kuhn, J. M. Castillo-Sanchez, J. Gascon, S. Calero, D. Dubbeldam, T. J. H. Vlugt, F. Kapteijn and J. Gross, *J. Phys. Chem. C*, 2009, **113**, 14290.